Available online at www.sciencedirect.com
SCIENCE DIRECT
Journal of Chemical Neuroanatomy 30 (2005) 119–128
Journal of CHEMICAL NEUROANATOMY
www.elsevier.com/locate/jchemneu

Differential effects on [^{35}S]GTPγS binding using muscarinic agonists and antagonists in the gerbil brain

Fuencisla Pilar-Cuéllar [a], Miguel Angel Paniagua [a], Ricardo Mostany [b], Carlos César Pérez [c], Arsenio Fernández-López [a,*]

[a] *Dpto. Biología Celular, Facultad de Ciencias Biológicas y Ambientales, Campus de Vegazana s/n, Universidad de León, 24071 León, Spain*
[b] *Dpto. Fisiología y Farmacología, Facultad de Medicina, Herrera Oria s/n, 39011 Santander, Cantabria, Spain*
[c] *Dpto. Medicina Veterinaria, Facultad de Veterinaria, Campus de Vegazana s/n, 24071 León, Spain*

Received 8 July 2004; received in revised form 16 June 2005; accepted 17 June 2005
Available online 10 August 2005

Abstract

In this work, we studied the in vitro G-protein activation induced by muscarinic agonists using [^{35}S]guanylyl-5′-*O*-(γ-thio)-triphosphate ([^{35}S]GTPγS) autoradiographic methods to characterize the M_2 and M_4 muscarinic subtypes response. Thus, we describe a detailed characterization of the increases in [^{35}S]GTPγS binding elicited by carbachol (Cch) and oxotremorine (OXO) (binding in the presence minus binding in the absence of agonist) throughout the gerbil brain (*Meriones unguiculatus*). For both agonists, the strongest stimulations were found in the superficial gray layer of the superior colliculus, the anteroventral and anteromedial thalamic nuclei, the anterior paraventricular thalamic nucleus, and the caudate-putamen. The comparative study using OXO and Cch suggested that OXO is able to detect differences in the response of structures enriched in M_4 muscarinic receptors, showing a lower potency to stimulate these brain areas. Furthermore, using increasing concentrations of selective M_2 (AF-DX 116) and M_1/M_4 (pirenzepine) antagonists to inhibit specific Cch- or OXO-induced [^{35}S]GTPγS binding, significant differences were observed in M_2-enriched structures but not in M_4-enriched ones such as the caudate-putamen. These data indicate that appropriate muscarinic agonist stimulation, together with selective inhibition of this effect using functional autoradiography, can be used as a tool to unravel the M_2- and M_4-muscarinic subtype-mediated response.

Keywords: M_2; M_4; Functional autoradiography; Carbachol; Oxotremorine; Pirenzepine

1. Introduction

Acetylcholine muscarinic receptors are widely distributed throughout the organism. In the central nervous system (CNS), they are involved in motor control, temperature regulation, cardiovascular regulation, and memory (Caulfield and Birdsall, 1998). They are also implicated in the pathophysiology of neurodegenerative diseases such as Alzheimer's and Parkinson's (Cowburn et al., 1996; Piggott et al., 2003).

Muscarinic receptors belong to the superfamily of proteins with seven transmembrane-spanning domains (Felder, 1995). The interaction with a specific agonist induces conformational changes within the receptor, promoting the activation of an associated G-protein, and subsequent dissociation of the α and βγ subunits of the G-protein (Gilman, 1987; Birnbaumer et al., 1990). Both the α and βγ subunits are able to interact with different signal transduction pathways (Neer, 1995; Clapham and Neer, 1997). Five muscarinic receptors have been described: M_1–M_5. The M_1, M_3 and M_5 subtypes are coupled to pertussis toxin-insensitive G-proteins ($G_{q/11}$), which stimulate phospholipases A2, C and D (Conklin et al., 1988; Peralta et al., 1988; Sandmann et al., 1991). The M_2 and M_4 subtypes are coupled to pertussis toxin-sensitive G-proteins ($G_{i/o}$), thus inhibiting adenylyl cyclase activity (Peralta et al., 1988).

The main problem in characterizing the muscarinic receptors is the low specificity of their ligands, which does not permit a clear discrimination among subtypes. This

* Corresponding author. Tel.: +34 987 29 14 85; fax: +34 987 29 12 76.
E-mail address: dbcafl@unileon.es (A. Fernández-López).

0891-0618/$ – see front matter © 2005 Elsevier B.V. All rights reserved.
doi:10.1016/j.jchemneu.2005.06.004

problem is especially important in the CNS where the involvement of a mixture of subtypes results in a confusing pharmacological profile, which may account for many of the controversies appearing in the literature (Caulfield and Birdsall, 1998). Therefore, the use of techniques that allow the study of only a number of muscarinic subtypes will simplify the problem. In this regard, a more selective approach to study M_2 and M_4 receptors has appeared over the past decade, where an autoradiographic method for studying the activation of $G_{i/o}$ protein-coupled receptors within the different structures in the brain has been developed (Sim et al., 1995). This method is based on the use of [^{35}S]guanylyl-5′-*O*-(γ-thio)-triphosphate ([^{35}S]GTPγS), a poorly hydrolysable GTP analogue, which is exchanged for GDP when the receptor is activated (Sim et al., 1995, 1996, 1997a, 1997b). Recently, Laitinen (1999) used different approaches to reduce [^{35}S]GTPγS binding in the absence of agonists (basal binding), including adenosine deaminase (ADA), and Moore et al. (2000) used ADA in their protocol as a routine way of eliminating the effect of endogenous adenosine, which strongly increases basal binding.

A number of reports have described stimulation by carbachol (Cch) in some brain structures in humans and rats (Capece et al., 1998; Rodríguez-Puertas et al., 2000; Demarco et al., 2003). However, no detailed studies have been carried out on this agonist-stimulated [^{35}S]GTPγS binding technique, commonly known as functional autoradiography, throughout the mammalian brain. Previous reports assessing [^{35}S]GTPγS binding to membrane homogenates indicated that Cch induces a stronger response than oxotremorine (OXO) in the rat olfactory bulb (Olianas and Onali, 1996). A similar response was observed in studies assessing adenylyl cyclase inhibition in the caudate-putamen (McKinney et al., 1991).

The Mongolian gerbil (*Meriones unguiculatus*) is known to have genetically determined susceptibility to seizures (Loskota et al., 1974) that can be elicited by simple external stimuli (Ludvig et al., 1991) and we have previously described that this species presents a seizure-refractory period after a single stimulation and inhibition of seizures after repetitive stimulation (Revilla et al., 1999). Using functional autoradiography to characterize the muscarinic receptors in this species, we unexpectedly found that the response elicited by non specific muscarinic agonists were different among muscarinic-enriched brain areas. Thus, we describe for the first time a comparative characterization study of OXO- and Cch-induced [^{35}S]GTPγS binding stimulation (binding in the presence minus binding in the absence of agonist) in the male gerbil brain, using functional autoradiographic assays. Although Cch and OXO are M_2 rather than M_4 selective agonists, they show some differences in their M_2 affinities in recombinant receptor studies (Dong et al., 1995). For this reason, in the present study, detailed inhibition studies of OXO- and Cch-mediated stimulation were carried out using selective M_2 and M_4 antagonists as inhibitors. We observed for the first time that caudate-putamen, an M_4 enriched structure, exhibits a differential response with respect to other M_2-enriched brain structures.

2. Materials and methods

All animals used in this study were treated in accordance with the European Communities Council Directive of 24 November 1986 (86/609/EEC) on the care and use of animals in scientific research and the NIH Office of Animal Care and Use (OACU) guidelines (http://oacu.od.nih.gov/). The experimental protocol was approved by the University of León's Ethics Committee.

To avoid possible variability induced in females by changes in hormonal levels in the different stages of their estral cycle (Lovel, 1986), five male 6-month-old gerbils (*Meriones unguiculatus*, 63.3 ± 3.7 g weight) were used. The animals were individually housed at 20 °C under standard conditions—12 h light and 55% humidity—and fed with the A04 (UAR, Epiny sur Orge, France) maintenance rat diet and water ad libitum. The animals were decapitated, and their brains were rapidly removed, frozen in liquid nitrogen, and stored at −80 °C until used. Additionally to the studies performed in the gerbil, in order to have our own rodent muscarinic receptor distribution data in rodents other than those of the literature, parallel quantitative autoradiographic studies were carried out with five 6-month-old male rats (*Rattus norvegicus*) and with five 6-month-old male mice (*Mus musculus*).

2.1. Functional autoradiographic studies

Serial coronal 10 μm thick brain sections were obtained with a cryostat, mounted onto silanized slides, and stored at −80 °C until used but not for longer than 15 days of storage. The autoradiographs corresponding to muscarinic agonist-stimulated [^{35}S]GTPγS binding sites were obtained following the initial functional autoradiography protocol (Sim et al., 1995), modified to include adenosine deaminase (ADA) (Moore et al., 2000). Thus, slides were incubated for 30 min at room temperature in 50 mM Tris–HCl buffer, pH 7.7, containing 3 mM $MgCl_2$, 0.2 mM EGTA, 100 mM NaCl, 1 mM DTT and 2 mM GDP. Then, the slides were incubated for 120 min at room temperature in the same buffer containing 3 mU/ml ADA and 0.05 nM [^{35}S]GTPγS (1250 Ci/mmol) to determine basal activity (basal binding). Different concentrations of Cch (100 nM–1 mM) and OXO (300 pM–30 μM) were used to characterize muscarinic receptor-coupled G protein activation (total binding).

The specificity of the muscarinic effect was assessed by inhibiting agonist stimulation with 1 μM atropine, a non-selective muscarinic antagonist. Non-specific binding was defined by incubating consecutive sections under the same conditions in the presence of 10 μM unlabelled GTPγS.

The preferent M_2- or M_4-mediated stimulation was assessed by inhibiting the stimulation obtained with 100 μM

Cch and 3 μM OXO [^{35}S]GTPγS binding with a range of increasing concentrations of AF-DX 116 (10 nM–100 μM), an M_2 selective antagonist ($pK_{IM2} = 6.73$) (Buckley et al., 1989), and of pirenzepine (10 nM–1 mM), an M_1/M_4 selective antagonist ($pK_{IM1} = 8.2$, $pK_{IM4} = 7.43$) (Dörje et al., 1991).

After incubation, the slides were washed twice with ice-cold 50 mM Tris–HCl buffer, pH 7.4, and once in ice-cold distilled water. The slides were then dried in a cold air stream and exposed to Kodak Biomax-MR film (Amersham) together with ^{14}C radioactive microscales for 4 days to generate the autoradiographs. The optical densities of the autoradiographs were measured using specific image analysis software (Scion Image, Scion Co) and converted to nCi/g tissue using a second-order polynomial equation whose parameters were obtained from a non-linear regression correlating nCi/g tissue from the ^{14}C radioactive microscales (provided by the manufacturer) with the corresponding optical densities (measured under the same conditions as the autoradiograph).

The maximum stimulation effect (E_{max}) and the 50% effective concentration (EC_{50}) were obtained using the GraphPad Prism, version 4.00, for Windows. Statistical analyses to compare the stimulation response (E_{max} and pEC_{50}) in each structure between Cch and OXO, as well as the inhibitory effect (pIC_{50}) between the AF-DX 116 and pirenzepine, were performed using paired *t*-tests. One-way ANOVA analysis, followed by a Student–Newman–Keuls test, were performed to compare the pEC_{50} values for Cch and OXO, and the pIC_{50} values for AF and Pz among the different brain structures studied. All statistical analyses were made using SPSS version 9.0 for Windows. For statistical analyses, two significant figures (decimals) were used for the pIC_{50} and pEC_{50} values.

2.2. Quantitative autoradiographic studies

Coronal 10 μm thick brain sections consecutive to those used in functional autoradiography were obtained with a cryostat, mounted on silanized slides, and stored at −80 °C until used. The protocol used for the autoradiographic localization of muscarinic receptors was that described by Cortés et al. (1984), with minimal modifications. Briefly, slides were incubated in 0.5 nM [^{3}H]NMS (79 Ci/mmol, Amersham) in 80 mM Na/K phosphate buffer, pH 7.4, for 60 min at room temperature. Non-specific binding was determined as that remaining in the presence of 1 μM atropine. After the incubation period, slides were rinsed in the same buffer at 4 °C, washed twice for 5 min in cold buffer, and rinsed again in cold distilled water. Autoradiographs were generated by exposing the slides with the labelled tissue sections to tritium-sensitive film ([^{3}H]Hyperfilm, Amersham) for 15 days together with the appropriate radioactive standards, after which they were developed using standard procedures. The autoradiographs were finally analysed and quantified using a computer-assisted image analysis system (Scion Image) to measure film optical densities, and densitometric readings were converted into values of tissue-bound radioligand expressed in fmol radioligand/mg tissue using Prism 4.00 software.

3. Results

The autoradiographic values using [^{3}H]NMS as radioligand are shown in Table 1 as well as the relative values of the different structures studied compared to the outer layer of the frontoparietal somatosensorial cortex, which exhibited the highest [^{3}H]NMS binding value. High or very high binding values were found in the external and inner layer of the cingulate cortex, visual cortex, CA1 oriens, pyramidal, stratum radiatum and lacunosum moleculare layers of the hippocampus, dentate gyrus, superficial gray layer of the superior colliculus, anteroventral and anteromedial thalamic nuclei, primary motor cortex, intermediate and inner layers of the frontoparietal somatosensorial cortex, and caudate-putamen. The remaining structures displayed moderate or low [^{3}H]NMS binding values (Table 1). No differences in the [^{3}H]NMS binding distribution were observed among rat, mouse and gerbil.

Concentration–response curves for the values of [^{35}S]GTPγS binding induced by different concentrations of Cch (100 nM to 1 mM) and OXO (300 pM to 30 μM) in several brain structures are shown in Fig. 1, where a plateau can be observed for OXO in the micromolar range and for

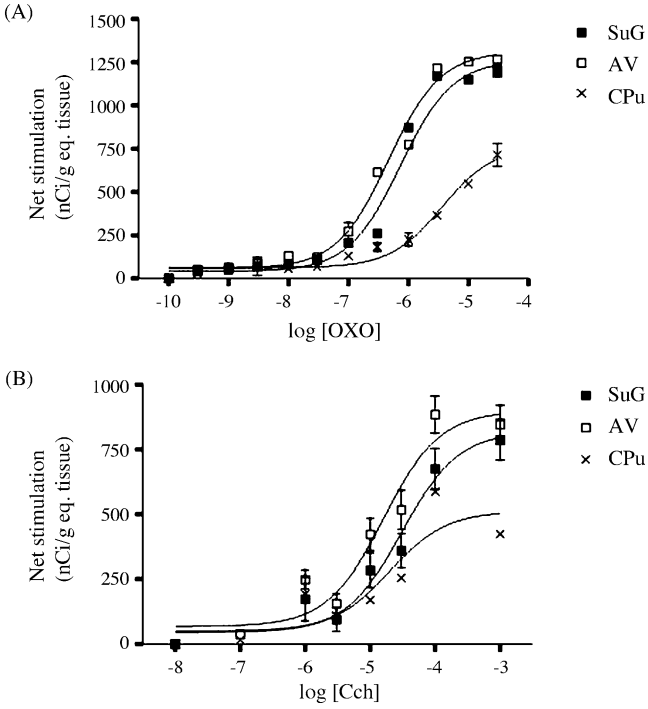

Fig. 1. Net stimulation of [^{35}S]GTPγS binding induced by a range of concentrations of the agonists OXO (A) and Cch (B) in different structures of the gerbil brain. AV: anteroventral thalamic nucleus, CPu: caudate-putamen and SuG: superficial gray layer of the superior colliculus.

Table 1
[^{3}H]NMS binding values for the labelling of total number of muscarinic receptors in different structures throughout the gerbil brain

	Mean ± S.E.M.	
Granular layer of the cerebellum	35 ± 2	L
Molecular layer of the cerebellum	17 ± 1	L
Cingulate cortex, outer layer	180 ± 12	H
Cingulate cortex, intermediate layer	138 ± 10	M
Cingulate cortex, inner layer	243 ± 20	H
Visual cortex, outer layer	264 ± 17	VH
Visual cortex, intermediate layer	217 ± 14	H
Visual cortex, inner layer	219 ± 16	H
CA1 oriens layer of the hippocampus	231 ± 17	H
CA1 pyramidal cell layer of the hippocampus	217 ± 16	H
CA1 stratum radiatum of the hippocampus	202 ± 18	H
CA1 lacunosum moleculare layer of the hippocampus	176 ± 15	H
Dentate gyrus	252 ± 24	H
Superficial gray layer of the superior colliculus	180 ± 14	H
Optic nerve layer of the superior colliculus	101 ± 3	L
Deep gray layer of the superior colliculus	91 ± 4	L
Medial geniculate nucleus, dorsal part	148 ± 8	M
Medial geniculate nucleus, medial part	110 ± 5	L
Medial geniculate nucleus, ventral part	148 ± 7	M
Dorsomedial periaqueductal gray	109 ± 5	L
Dorsolateral periaqueductal gray	113 ± 5	L
Anteroventral thalamic mucleus	263 ± 7	VH
Anteromedial thalamic mucleus	177 ± 4	H
Primary motor cortex, outer layer	256 ± 2	H
Primary motor cortex, intermediate layer	232 ± 18	H
Primary motor cortex, inner layer	272 ± 32	VH
Frontoparietal somatosensorial cortex, outer layer	341 ± 10	Max
Frontoparietal somatosensorial cortex, intermediate layer	262 ± 10	VH
Frontoparietal somatosensorial cortex, inner layer	276 ± 18	VH
Caudate-putamen	288 ± 16	VH

The binding values are expressed in fmol/mg tissue, as means ± S.E.M. Max indicates the highest density values; VH (very high binding) indicates relative values higher than 75% with respect to Max; H (high binding) indicates relative values ranging from 50 to 75% with respect to Max; M (moderate binding) indicates relative values ranging from 35 to 50% with respect to Max, and L indicates relative values lower than 35% with respect to Max, considered low or non-specific binding.

Cch in the millimolar range in most of the structures. The E_{max} and pEC_{50} values for several structures are shown in Table 2. EC_{50} values for OXO are in the micromolar range while those for Cch range around 30 μM. We failed to find significant differences in the pEC_{50} values for Cch among the different structures analyzed by one-way ANOVA analysis. Likewise, no significant differences in pEC_{50} values were detected for OXO in the different structures

Table 2
pEC_{50} and E_{max} values for [^{35}S]GTPγS binding stimulation by the muscarinic agonists Cch and OXO throughout the gerbil brain

	pEC_{50}			E_{max}		
	Cch (mean ± S.E.M.)	OXO (mean ± S.E.M.)	S	Cch (mean ± S.E.M.)	OXO (mean ± S.E.M.)	S
Cingulate cortex, inner layer	4.56 ± 0.1	6.16 ± 1.5		409 ± 18	407 ± 113	
Superficial gray layer of the superior colliculus	4.49 ± 0.1	5.93 ± 0.2		827 ± 77	785 ± 42	
Optic nerve layer of the superior colliculus	4.54 ± 0.1	5.89 ± 0.2	*	561 ± 67	614 ± 23	
Deep gray layer of the superior colliculus	4.43 ± 0.2	5.97 ± 0.2	*	423 ± 64	479 ± 65	
Medial geniculate nucleus, dorsal part	4.69 ± 0.2	6.86 ± 0.4	*	540 ± 81	359 ± 41	
Anterior pretectal nucleus	4.65 ± 0.2	6.05 ± 0.1	*	558 ± 53	446 ± 92	
Dorsomedial periaqueductal gray	4.46 ± 0.2	6.16 ± 0.2	*	368 ± 35	449 ± 11	
Dorsolateral periaqueductal gray	4.54 ± 0.1	6.23 ± 0.2	*	380 ± 45	423 ± 3	
Anteroventral thalamic nucleus	4.79 ± 0.1	6.10 ± 0.2	*	899 ± 84	866 ± 82	
Anteromedial thalamic nucleus	4.55 ± 0.1	5.83 ± 0.1	*	704 ± 32	643 ± 49	
Paraventricular thalamic nucleus	4.62 ± 0.3	5.80 ± 0.2	*	374 ± 11	557 ± 32	*
Medial preoptic area	4.57 ± 0.3	6.48 ± 1.5		274 ± 24	466 ± 21	
Caudate-putamen	4.58 ± 0.1	5.66 ± 0.2		512 ± 27	534 ± 51	

E_{max} values are expressed in nCi/g tissue. Both pEC_{50} ($-\log EC_{50}$) and E_{max} values are expressed as mean ± S.E.M. The table only shows the structures that presented the highest responses within the different areas analyzed of the brain, while others, such as different areas of the cortex, hippocampus and cerebellum that presented low responses, are not shown. Asterisks indicate structures showing significant differences ($p < 0.05$) in pEC_{50} and E_{max} values for Cch and OXO (paired *t*-test).

analyzed (one-way ANOVA). Upon searching for differences in the responses between OXO and Cch in each structure, OXO response values (pEC_{50}) were significantly higher than those of Cch (paired *t*-test) in most of the structures studied, except the inner layer of the cingulate cortex, the superficial gray layer of the superior colliculus, the medial preoptic area and the caudate-putamen (Table 2).

The anteroventral thalamic nucleus displayed the maximum E_{max} value for both Cch and OXO. The superficial gray layer and optic nerve layer of the superior colliculus, dorsal part of the medial geniculate nucleus, anterior pretectal nucleus, anteromedial and paraventricular thalamic nuclei and caudate-putamen exhibited high E_{max} values (>500 nCi/g equivalent tissue). Moderate E_{max} values (400–500 nCi/g equivalent tissue) were observed in the inner layer of the cingulate cortex, the deep gray layer of the superior colliculus, the dorsomedial and dorsolateral periaqueductal gray, the medial preoptic area and the septum. The remaining structures were considered to have low or non-specific stimulation. Regarding E_{max} values, only the paraventricular thalamic nucleus exhibited significant differences in the response to OXO versus Cch (paired *t*-test) (Table 2). Fig. 2 shows the

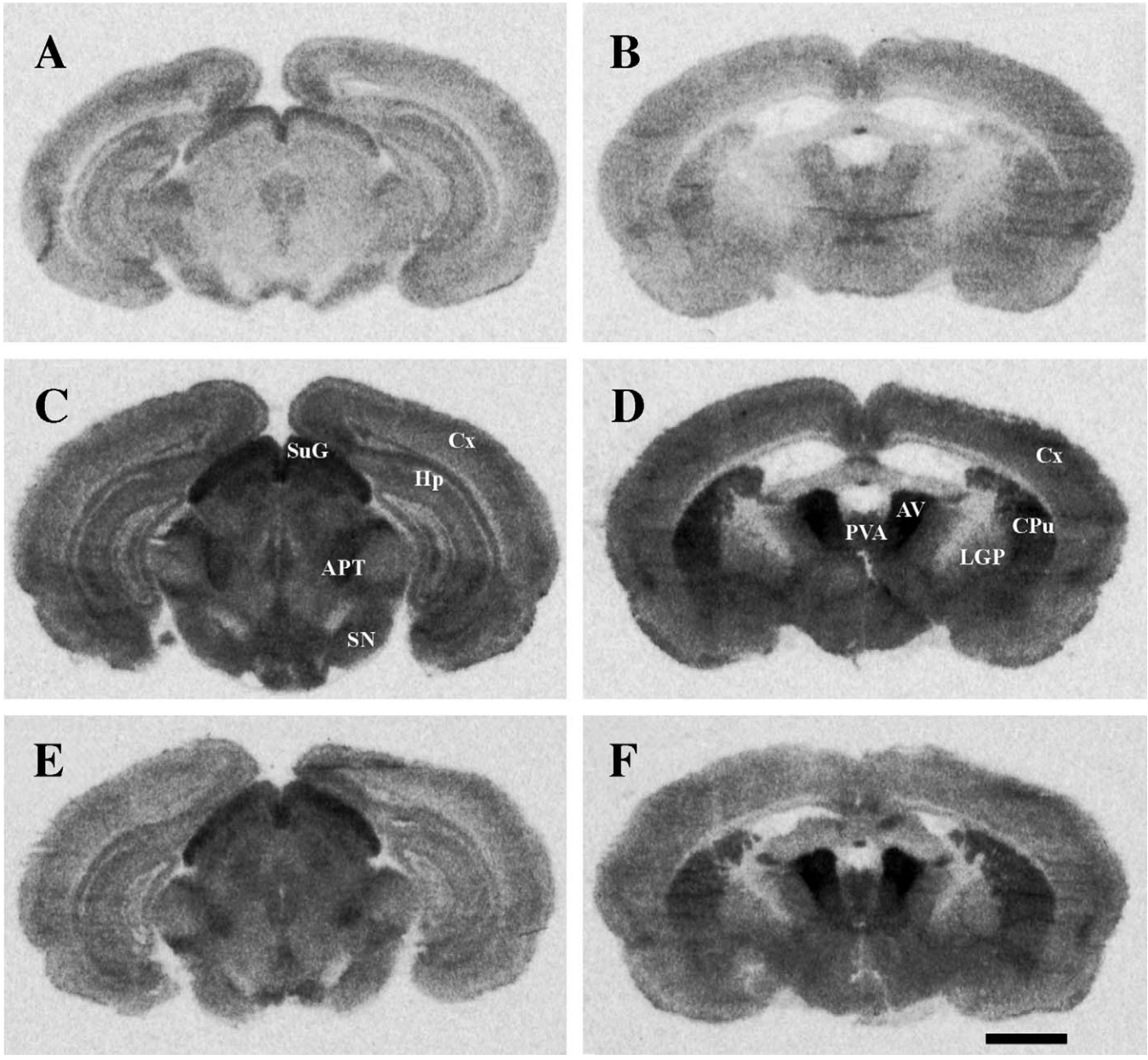

Fig. 2. Autoradiographic images of [^{35}S]GTPγS binding in the gerbil brain at two brain levels corresponding to the anterior pretectal nucleus (APT) (A, C, E) and the anteroventral thalamic nucleus (AV) (B, D, F). Basal binding (A, B); 100 μM Cch-stimulated [^{35}S]GTPγS binding (C, D) and 3 μM OXO-stimulated [^{35}S]GTPγS binding (E, F). CPu: caudate-putamen; Cx: cerebral cortex; Hp: hippocampus; LGP: lateral globus pallidus; PVA: paraventricular thalamic nucleus, anterior part; SN: substantia nigra; SuG: superficial gray layer of the superior colliculus. All images at same magnification. Bar: 2 mm.

Table 3
pIC_{50} values for the muscarinic antagonists pirenzepine (Pz) and AF-DX 116 (AF) after stimulation with 100 μM Cch and 3 μM OXO throughout the gerbil brain

	Cch			OXO			S	
	AF (mean ± S.E.M.)	Pz (mean ± S.E.M.)	S	AF (mean ± S.E.M.)	Pz (mean ± S.E.M.)	S	AF	PZ
Cingulate cortex, inner layer	5.29 ± 1.2	4.31 ± 0.9		8.63 ± 3.7	3.65 ± 0.1			
Superficial gray layer of the superior colliculus	5.73 ± 0.1	5.00 ± 0.3		5.17 ± 0.2	4.60 ± 0.1		*	
Optic nerve layer of the superior colliculus	5.85 ± 0.0	5.13 ± 0.2	*	5.43 ± 0.2	4.83 ± 0.0	*		
Deep gray layer of the superior colliculus	5.90 ± 0.1	5.23 ± 0.2	*	5.47 ± 0.2	4.78 ± 0.0			
Medial geniculate nucleus, dorsal part	5.02 ± 0.8	5.39 ± 0.2		4.57 ± 0.5	4.55 ± 0.1			
Anterior pretectal nucleus	5.82 ± 0.0	5.39 ± 0.2		5.49 ± 0.1	5.02 ± 0.1	*		
Dorsomedial periaqueductal gray	5.93 ± 0.2	5.16 ± 0.3		5.09 ± 0.2	4.55 ± 0.0	*		*
Dorsolateral periaqueductal gray	5.92 ± 0.2	5.20 ± 0.2	*	5.28 ± 0.2	4.81 ± 0.1			
Anteroventral thalamic nucleus	5.66 ± 0.1	4.99 ± 0.1	*	5.65 ± 0.1	4.94 ± 0.1	*		
Anteromedial thalamic nucleus	5.86 ± 0.1	4.63 ± 0.2		5.40 ± 0.2	6.13 ± 1.6			
Paraventricular thalamic nucleus	5.97 ± 0.3	4.23 ± 0.3	*	6.16 ± 1.3	4.58 ± 0.4			
Medial preoptic area	5.40 ± 0.5	4.86 ± 0.8		4.84 ± 0.4	4.45 ± 0.2			
Caudate-putamen	5.48 ± 0.1	5.69 ± 0.2		4.21 ± 0.5	4.48 ± 0.5			

Values are expressed as mean ± S.E.M. pIC_{50} values for Pz and AF-DX 116 were compared using a paired *t*-test (*$p < 0.05$).

stimulations obtained with 3 μM OXO and 100 μM Cch, whose values are similar to those of E_{max}.

Comparative studies using the antagonists AF-DX 116 and pirenzepine to inhibit Cch and OXO-induced [^{35}S]GTPγS stimulation were carried out throughout the gerbil brain. We failed to observe significant differences (one-way ANOVA analysis) upon comparing the pIC_{50} values of each antagonist for either the Cch or OXO-induced [^{35}S]GTPγS stimulation. However, upon comparing the pirenzepine and AF-DX 116 inhibitions to Cch-stimulated binding in each structure, we found significant differences (paired *t*-test) in a number of structures such as the optic nerve layer and deep gray layer of the superior colliculus, dorsolateral periaqueductal gray, anteroventral thalamic nucleus and paraventricular thalamic nucleus. Also, significant differences between pirenzepine and AF-DX 116 inhibitions to OXO-stimulated binding

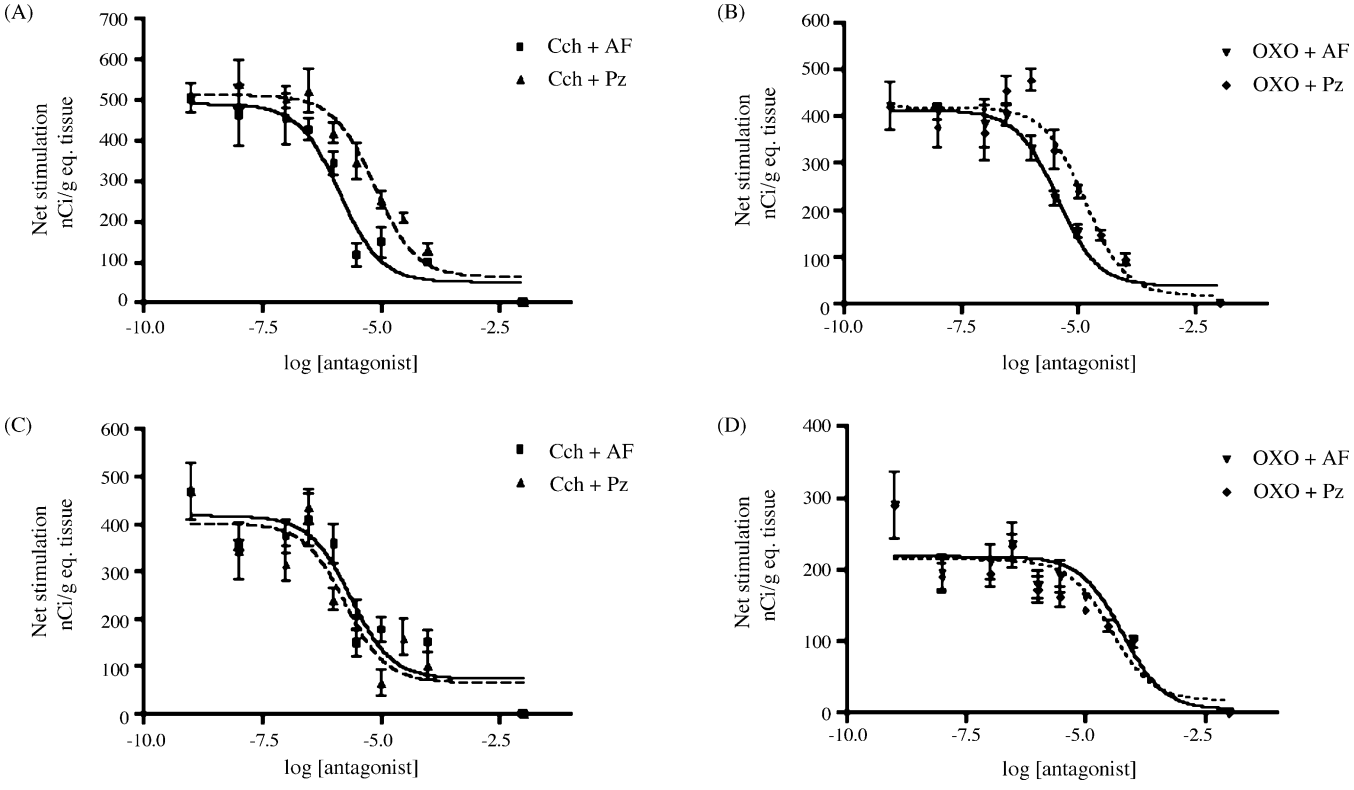

Fig. 3. Effect of increasing concentrations of the muscarinic antagonists AF-DX 116 (AF) (M_2 antagonist) and pirenzepine (Pz) (M_1/M_4 antagonist) on (A) 100 μM Cch-induced [^{35}S]GTPγS binding stimulation in the superior colliculus; (B) 3 μM OXO-induced [^{35}S]GTPγS binding stimulation in the superior colliculus; (C) 100 μM Cch-induced [^{35}S]GTPγS binding stimulation in the caudate-putamen and (D) 3 μM OXO-induced [^{35}S]GTPγS binding stimulation in the caudate-putamen.

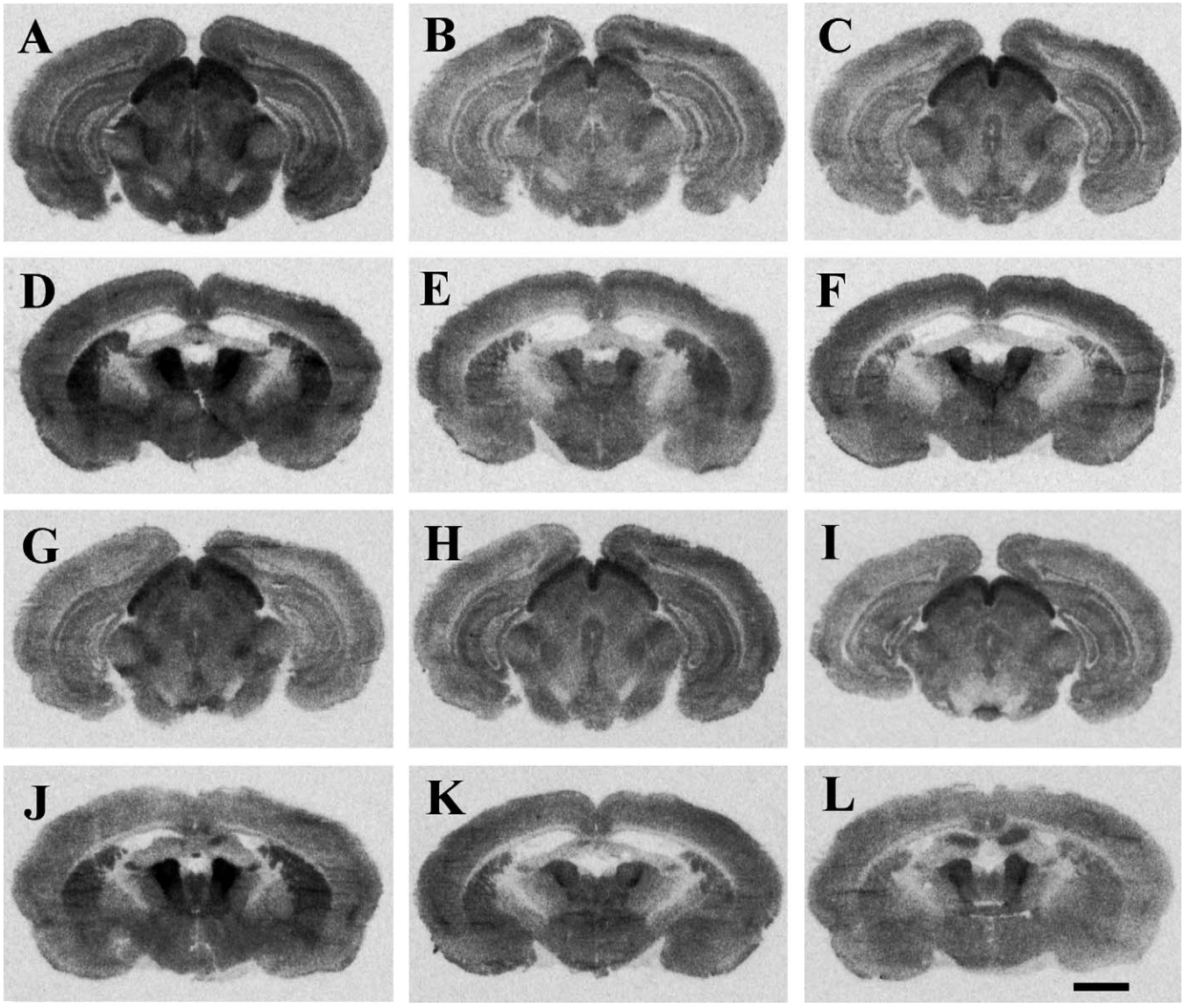

Fig. 4. Autoradiographic images of [^{35}S]GTPγS binding in the gerbil brain at two brain levels corresponding to the anterior pretectal nucleus (APT) (A, B, C, G, H, I) and the anteroventral thalamic nucleus (AV) (D, E, F, J, K, L). Figures (A) and (D) correspond to100 μM Cch-stimulated [^{35}S]GTPγS binding; (B) and (E) correspond to 100 μM Cch stimulation inhibited by 3 μM AF-DX 116, and (C) and (F) to 100 μM Cch stimulation inhibited by 10 μM pirenzepine. Figures (G) and (J) correspond to 3 μM OXO-stimulated [^{35}S]GTPγS binding; (H) and (K) to 3 μM OXO stimulation inhibited by 3 μM AF-DX 116, and (I) and (L) to 3 μM OXO stimulation inhibited by 10 μM pirenzepine. All images at same magnification. Bar: 2 mm.

appeared in optic nerve layer of the superior colliculus, anterior pretectal nucleus, dorsomedial periaqueductal gray and anteroventral thalamic nucleus (Table 3). Fig. 3 shows the inhibitory effects of increasing concentrations of AF-DX 116 and pirenzepine on the Cch- and OXO-induced [^{35}S]GTPγS stimulation in the caudate-putamen and superior colliculus, and Fig. 4 shows the inhibitory effect of a single concentration of these antagonists on both agonist-induced [^{35}S]GTPγS bindings. It must be pointed out that pIC_{50} values of antagonists have been estimated from a functional response, measured as [^{35}S]GTPγS binding, instead the classic pharmacological approach of measuring direct interactions between ligands and receptors. Since functional responses need of higher amounts of agonist, probably pIC_{50} values of antagonists are much higher than their actual potencies at these receptors because these values are determined not only by the potency of the antagonist but also by the concentration and affinity of the agonist used.

4. Discussion

4.1. [^{3}H]NMS binding distribution in autoradiographic assays

We carried out parallel autoradiographic assays in the rat, mouse and gerbil brain using Cch or OXO to induce [^{35}S]GTPγS binding. Also, parallel autoradiographic stu-

dies, in sections consecutive to those of the functional autoradiography, were performed in gerbils, mice and rats using [^{3}H]NMS in order to compare both receptor binding sites and receptor agonist response distributions. Moreover, the [^{3}H]NMS autoradiographic data were used to compare the distribution of muscarinic receptors in these rodents using this radioligand, since no previous data using this radioligand have been reported in gerbil brain. Our results in the quantitative autoradiography (Table 1) revealed a similar distribution in all three species, thus confirming data obtained in the rat (Cortés and Palacios, 1986a; Cortés et al., 1986b) and the previous report using [^{3}H]QNB in the gerbil (Hara et al., 1992).

4.2. Comparative study of [^{3}H]NMS binding and OXO- and Cch-stimulated [^{35}S]GTPγS binding throughout the gerbil brain

Comparison between the quantitative and functional autoradiographies showed that while [^{3}H]NMS binding values were very high in the dentate gyrus, stratum radiatum of the hippocampus, oriens layer of the hippocampus and cerebral cortical layers, these structures only showed moderate or low levels of Cch- or OXO-induced [^{35}S]GTPγS binding, indicating that in these areas the $M_1/M_3/M_5$ muscarinic receptor component predominates. This confirms the subtype distribution studies carried out by in situ hybridization (Buckley et al., 1988; Vilaró et al., 1994) and immunocytochemistry (Levey et al., 1991; Levey, 1993). Strikingly, the increase in Cch- or OXO-induced [^{35}S]GTPγS binding observed in these areas was not inhibited by generic antagonists such as atropine, the selective M_2 antagonist AF-DX 116 or the selective M_1/M_4 antagonist pirenzepine. Two conclusions can be derived from these data: first, that functional autoradiographic assays are not able to detect the M_2/M_4 response in these areas (and hence were not included in our results) and second, that the specificity of the response must be checked by using antagonists in order to avoid misinterpretations regarding the agonist-induced stimulation following this technique.

Other structures, such as the superior colliculus, caudate-putamen and anterior thalamic nuclei, displayed high Cch- and OXO-induced [^{35}S]GTPγS binding values. These data parallel those obtained from [^{3}H]NMS (Table 1) or [^{3}H]QNB (Hara et al., 1992) autoradiographic binding experiments. We wish to emphasise the very strong stimulations of two structures, the anteroventral and anteromedial thalamic nuclei, which, together with the superior colliculus, showed the maximum net stimulation induced by the Cch and OXO agonists. The stimulation of these nuclei was completely inhibited by the antagonists atropine, AF-DX 116 and pirenzepine, indicating their M_2/M_4 muscarinic receptor nature. The Cch- or OXO-induced [^{35}S]GTPγS binding parallels the results of in situ hybridization studies of the distribution of M_2/M_4 receptors in the rat (Buckley et al., 1988; Vilaró et al., 1994) as well as the [^{3}H]AF-DX 116 (Regenold et al., 1989) and [^{3}H]AF-DX 384 (Aubert et al., 1992) binding distributions reported for the rat, thus confirming the M_2/M_4 muscarinic receptor distribution in rodents. Also, using functional autoradiography (Rodríguez-Puertas et al., 2000) in humans some of these areas—such as the striatum—have been described to show a high degree of stimulation with Cch.

4.3. Distribution of OXO- and Cch-stimulated [^{35}S]GTPγS binding throughout the gerbil brain

The [^{35}S]GTPγS binding values obtained following incubation with different concentrations of OXO or Cch as agonists indicate that their optimum concentrations to stimulate muscarinic receptors are in the micromolar range for OXO and in the submillimolar range for Cch, since higher concentrations of these agonists failed to induce higher stimulations. Analysis of [^{35}S]GTPγS stimulation curves indicates that OXO is significantly more potent than Cch in inducing muscarinic-mediated stimulation in most of the structures studied.

The Cch pEC_{50} values were similar in all the structures studied and similar OXO pEC_{50} values were also found in most structures studied, except the caudate-putamen. Upon comparing the pEC_{50} values for both agonists, OXO displayed a 10–100-fold higher potency than Cch in most structures. Nevertheless, some structures, such as the caudate-putamen, an M_4-enriched area (Vilaró et al., 1991; Yasuda et al., 1993; Onali and Olianas, 2002; Piggott et al., 2002), did not show differences between the Cch and OXO pEC_{50} values. These results suggest a lower potency of OXO for M_4 than for M_2 muscarinic receptors, which is in agreement with previous reports indicating a lower potency of OXO for M_4 than for the M_2 subtype in adenylyl cyclase inhibition assays (McKinney et al., 1991). These data support the idea that comparative studies with both agonists would be useful to gain insight into the differences in the muscarinic M_2 or M_4 response throughout the brain.

4.4. Differential inhibition of M_2/M_4 agonist-induced [^{35}S]GTPγS binding using the selective antagonists AF-DX 116 and pirenzepine

Further assays inhibiting the stimulation of OXO and Cch with increasing concentrations of AF-DX 116 or pirenzepine revealed different types of behaviour in the inhibition curves, as shown in Fig. 3. Thus, while in most structures AF-DX 116 had significant higher pIC_{50} values than those of the pirenzepine in inhibiting both Cch and OXO stimulation, no differences were observed in the caudate-putamen. These data point to differences in the response of different brain structures reported to have different muscarinic M_2/M_4 ratios that can be unmasked by the combined effect of these ligands in functional autoradiography.

In the rat, the caudate-putamen has been reported to present higher $M_2 + M_4$ muscarinic receptor densities than the superior colliculus or the anteroventral thalamic nucleus (Smith et al., 1991). However, in our study we found a lower degree of stimulation in the caudate-putamen than in the superior colliculus or the anteroventral thalamic nucleus, confirmed using both agonists. Studies with recombinant receptors indicate that both Cch and OXO show higher affinities for M_2 than for M_4 (Dong et al., 1995). Furthermore, studies in other vertebrate species such as the chicken report similar results (Tietje et al., 1990; Tietje and Nathanson, 1991). The areas reported to display a predominance of M_4 over the M_2 muscarinic subtype, such as the caudate-putamen (Vilaró et al., 1991; Yasuda et al., 1993; Onali and Olianas, 2002; Piggott et al., 2002), the olfactory bulb (Olianas and Onali, 1991) and the olfactory tubercle (Vilaró et al., 1991; Yasuda et al., 1993) showed poorer stimulation using both agonists than those with a predominance of M_2, even when the total amounts of M_2 and M_4 muscarinic receptors are higher than those observed in predominantly M_2 structures. These observations are consistent with the pharmacology described for these ligands in the above-mentioned recombinant studies (Dong et al., 1995) and indicate that in native receptors Cch- and OXO-induced [^{35}S]GTPγS binding is more predominantly mediated by M_2 than by M_4 subtypes or that the efficacy of the stimulation is higher by M_2 than by M_4 muscarinic receptors. This would be in agreement with data indicating that M_2 receptors are able to bind to both α_{i1} and α_{i2} and both the α_{o1} and α_{o2} isoforms of the G protein, while M_4 is only able to bind to the α_{i2} and α_{o1} and α_{o2} isoforms (Migeon et al., 1995). Thus, not only the abundance but differences in the G protein coupling could be responsible for the more efficient response of M_2.

In brief, a major problem in the pharmacological characterization of muscarinic receptor subtypes is the lack of specific ligands, and this study shows that performing inhibition curves of the muscarinic stimulation using selective M_2 and M_4 antagonists, in functional autoradiography, provides a tool able to discriminate between the M_2- and M_4-subtype-mediated response.

Acknowledgments

This work has been supported by SAF2002-00292. We wish to thank to Rebeca Díez-Alarcia, María Rehberger and Susana Fernández Ibán for their support.

References

Aubert, I., Cecyre, D., Gauthier, S., Quirion, R., 1992. Characterization and autoradiographic distribution of [^{3}H]AF-DX 384 binding to putative muscarinic M_2 receptors in the rat brain. Eur. J. Pharmacol. 217, 173–184.

Birnbaumer, L., Abramowitz, J., Brown, A.M., 1990. Receptor-effector coupling by G proteins. Biochim. Biophys. Acta. 1031, 163–224.

Buckley, N.J., Bonner, T.I., Brann, M.R., 1988. Localization of a family of muscarinic receptor mRNAs in rat brain. J. Neurosci. 8, 4646–4652.

Buckley, N.J., Bonner, T.I., Buckley, C.M., Brann, M.R., 1989. Antagonist binding properties of five cloned muscarinic receptors expressed in CHO-K1 cells. Mol. Pharmacol. 35, 469–476.

Capece, M.L., Baghdoyan, H.A., Lydic, R., 1998. Carbachol stimulates [^{35}S]guanylyl 5′-(γ-thio)-triphosphate binding in rapid eye movement sleep-related brainstem nuclei of rat. J. Neurosci. 18, 3779–3785.

Caulfield, M.P., Birdsall, N.J., 1998. International Union of Pharmacology. XVII. Classification of muscarinic acetylcholine receptors. Pharmacol. Rev. 50, 279–290.

Clapham, D.E., Neer, E.J., 1997. G protein βγ subunits. Annu. Rev. Pharmacol. Toxicol. 37, 167–203.

Conklin, B.R., Brann, M.R., Buckley, N.J., Ma, A.L., Bonner, T.I., Axelrod, J., 1988. Stimulation of arachidonic acid release and inhibition of mitogenesis by cloned genes for muscarinic receptor subtypes stably expressed in A9 L cells. Proc. Natl. Acad. Sci. U.S.A. 85, 8698–8702.

Cortés, R., Probst, A., Palacios, J.M., 1984. Quantitative light microscopic autoradiographic localization of cholinergic muscarinic receptors in the human brain: brainstem. Neuroscience 12, 1003–1026.

Cortés, R., Palacios, J.M., 1986a. Muscarinic cholinergic receptor subtypes in the human brain. I. Quantitative autoradiographic studies. Brain Res. 362, 227–238.

Cortés, R., Probst, A., Tobler, H.J., Palacios, J.M., 1986b. Muscarinic cholinergic receptor subtypes in the human brain. II. Quantitative autoradiographic studies. Brain Res. 362, 239–253.

Cowburn, R.F., Wiehager, B., Ravid, R., Winblad, B., 1996. Acetylcholine muscarinic M2 receptor stimulated [^{35}S]GTPγS binding shows regional selective changes in Alzheimer's disease postmortem brain. Neurodegeneration 5, 19–26.

Demarco, G.J., Baghdoyan, H.A., Lydic, R., 2003. Differential cholinergic activation of G proteins in rat and mouse brainstem: relevance for sleep and nociception. J. Comp. Neurol. 457, 175–184.

Dong, G.Z., Kameyama, K., Rinken, A., Haga, T., 1995. Ligand binding properties of muscarinic acetylcholine receptor subtypes (m1–m5) expressed in baculovirus-infected insect cells. J. Pharmacol. Exp. Ther. 274, 378–384.

Dörje, F., Wess, J., Lambrecht, G., Tacke, R., Mutschler, E., Brann, M.R., 1991. Antagonist binding profiles of five cloned human muscarinic receptor subtypes. J. Pharmacol. Exp. Ther. 256, 727–733.

Felder, C.C., 1995. Muscarinic acetylcholine receptors: signal transduction through multiple effectors. FASEB J. 9, 619–625.

Gilman, A.G., 1987. G proteins: transducers of receptor-generated signals. Annu. Rev. Biochem. 56, 615–649.

Hara, H., Onodera, H., Kato, H., Kogure, K., 1992. Effects of aging on signal transmission and transduction systems in the gerbil brain: morphological and autoradiographic study. Neuroscience 46, 475–488.

Laitinen, J.T., 1999. Selective detection of adenosine A1 receptor-dependent G-protein activity in basal and stimulated conditions of rat brain [^{35}S]Guanosine 5′-(γ-thio)triphosphate autoradiography. Neuroscience 90, 1265–1279.

Levey, A.I., Kitt, C.A., Simonds, W.F., Price, D.L., Brann, M.R., 1991. Identification and localization of muscarinic acetylcholine receptor proteins in brain with subtype-specific antibodies. J. Neurosci. 11, 3218–3226.

Levey, A.I., 1993. Immunological localization of m1–m5 muscarinic acetylcholine receptors in peripheral tissues and brain. Life Sci. 52, 441–448.

Loskota, W.J., Lomax, P., Rich, S.T., 1974. The gerbil as a model for the study of the epilepsies. Epilepsia 15, 109–119.

Lovel, D.P., 1986. Variation in pentobarbitone sleeping time in mice 1. Strain and sex differences. Lab. Anim. 20, 85–90.

Ludvig, N., Farias, P.A., Ribak, C.E., 1991. An analysis of various environmental and specific sensory stimuli on the seizure of the Mongolian gerbil. Epilepsy Res. 8, 30–35.

McKinney, M., Miller, J.H., Gibson, V.A., Nickelson, L., Aksoy, S., 1991. Interactions of agonists with M2 and M4 muscarinic receptor sub-

types mediating cyclic AMP inhibition. Mol. Pharmacol. 40, 1014–1022.

Migeon, J.C., Thomas, S.L., Nathanson, N.M., 1995. Differential coupling of m2 and m4 muscarinic receptors to inhibition of adenylyl cyclase by $G_i\alpha$ and $G_o\alpha$ subunits. J. Biol. Chem. 270, 16070–16074.

Moore, R.J., Xiao, R., Sim-Selley, L.J., Childers, S.R., 2000. Agonist-stimulated [^{35}S]GTPγS binding in brain modulation by endogenous adenosine. Neuropharmacology 39, 282–289.

Neer, E.J., 1995. Heterotrimeric G proteins: organizers of transmembrane signals. Cell 80, 249–257.

Olianas, M.C., Onali, P., 1991. Muscarinic stimulation of adenylate cyclase activity of rat olfactory bulb.II. Characterization of the antagonist sensitivity and comparison with muscarinic inhibitions of the enzyme in striatum and heart. J. Pharmacol. Exp. Ther. 259, 680–686.

Olianas, M.C., Onali, P., 1996. Stimulation of guanosine 5′-O-(3-[^{35}S] thiotriphosphate) binding by cholinergic muscarinic receptors in membranes of rat olfactory bulb. J. Neurochem. 67, 2549–2556.

Onali, P., Olianas, M.C., 2002. Muscarinic M_4 receptor inhibition of dopamine D1-like receptor signalling in rat nucleus accumbens. Eur. J. Pharmacol. 448, 105–111.

Peralta, E.G., Ashkenazi, A., Winslow, J.W., Ramachandran, J., Capon, D.J., 1988. Differential regulation of PI hydrolysis and adenylyl cyclase by muscarinic receptor subtypes. Nature 334, 434–437.

Piggott, M., Owens, J., O'Brien, J., Paling, S., Wyper, D., Fenwick, J., Johnson, M., Perry, R., Perry, E., 2002. Comparative distribution of binding of the muscarinic receptor ligands pirenzepine, AF-DX 384, (R,R)-I-QNB and (R,S)-I-QNB to human brain. J. Chem. Neuroanat. 24, 211–223.

Piggott, M.A., Owens, J., O'Brien, J., Colloby, S., Fenwick, J., Wyper, D., Jaros, E., Johnson, M., Perry, R.H., Perry, E.K., 2003. Muscarinic receptors in basal ganglia in dementia with Lewy bodies. Parkinson's disease and Alzheimer's disease. J. Chem. Neuroanat. 25, 161–173.

Regenold, W., Araujo, D.M., Quirion, R., 1989. Quantitative autoradiographic distribution of [^{3}H]AF-DX 116 muscarinic-M_2 receptor binding sites in rat brain. Synapse 4, 115–125.

Revilla, V., Robles, M.S., Bermejo, J.C., Paniagua, M.A., Fernández-López, A., 1999. Seizure-refractory period after a single stimulation and inhibition of seizures after repetitive stimulation in the gerbil: effects on blood cortisol levels. Epilepsia 40, 1–4.

Rodríguez-Puertas, R., González-Maeso, J., Meana, J.J., Pazos, A., 2000. Autoradiography of receptor-activated G-proteins in post mortem human brain. Neuroscience 96, 169–180.

Sandmann, J., Peralta, E.G., Wurtman, R.J., 1991. Coupling of transfected muscarinic acetylcholine receptor subtypes to phospholipase D. J. Biol. Chem. 266, 6031–6034.

Sim, L.J., Selley, D.E., Childers, S.R., 1995. In vitro autoradiography of receptor-activated G proteins in rat brain by agonist-stimulated guanylyl 5′-[γ-[^{35}S]thio]-triphosphate binding. Proc. Natl. Acad. Sci. USA 92, 7242–7246.

Sim, L.J., Hampson, R.E., Deadwyler, S.A., Childers, S.R., 1996. Effects of chronic treatment with delta9-tetrahydrocannabinol on cannabinoid-stimulated [^{35}S]GTPγS autoradiography in rat brain. J. Neurosci. 16, 8057–8066.

Sim, L.J., Selley, D.E., Childers, S.R., 1997a. Autoradiographic visualization in brain of receptor-G protein coupling using [^{35}S]GTPγS binding. Methods Mol. Biol. 83, 117–132.

Sim, L.J., Xiao, R., Childers, S.R., 1997b. In vitro autoradiographic localization of 5-HT_{1A} receptor-activated G-proteins in the rat brain. Brain Res. Bull. 44, 39–45.

Smith, T.D., Annis, S.J., Ehlert, F.J., Leslie, F.M., 1991. N-[^{3}H]methylscopolamine labeling of non-M_1, non-M_2 muscarinic receptor binding sites in rat brain. J. Pharmacol. Exp. Ther. 256, 1173–1181.

Tietje, K.M., Goldman, P.S., Nathanson, N.M., 1990. Cloning and functional analysis of a gene encoding a novel muscarinic acetylcholine receptor expressed in chick heart and brain. J. Biol. Chem. 265, 2828–2834.

Tietje, K.M., Nathanson, N.M., 1991. Embryonic chick heart expresses multiple muscarinic acetylcholine receptor subtypes. Isolation and characterization of a gene encoding a novel m2 muscarinic acetylcholine receptor with high affinity for pirenzepine. J. Biol. Chem. 266, 17382–17387.

Vilaró, M.T., Wiederhold, K.H., Palacios, J.M., Mengod, G., 1991. Muscarinic cholinergic receptors in the rat caudate-putamen and olfactory tubercle belong predominantly to the m4 class: in situ hybridization and receptor autoradiography evidence. Neuroscience 40, 159–167.

Vilaró, M.T., Palacios, J.M., Mengod, G., 1994. Multiplicity of muscarinic autoreceptor subtypes? Comparison of the distribution of cholinergic cells and cells containing mRNA for five subtypes of muscarinic receptors in the rat brain. Brain Res. Mol. Brain Res. 21, 30–46.

Yasuda, R.P., Ciesla, W., Florres, L.R., Wall, S.J., Li, M., Satkus, S.A., Weissten, J.S., Spagnola, B.V., Wolfe, B.B., 1993. Development of antisera selective for m4 and m5 muscarinic cholinergic receptors: distribution of m4 and m5 receptors in rat brain. Mol. Pharmacol. 43, 149–157.